IMPULSE FACILITY SIMULATION OF HYPERVELOCITY RADIATING FLOWS

R. G. Morgan[1], T. J. McIntyre[1], P. A. Jacobs[1], D. R. Buttsworth[2], M. N. Macrossan[1], R. J. Gollan[1], B. R. Capra[1], A. M. Brandis[1], D. Potter[1], T. Eichmann[1], C. M. Jacobs[1], M. McGilvray[1], D. van Diem[1], and M. P. Scott[1]

[1]*Centre for Hypersonics, The University of Queensland, Brisbane 4072, Australia*
[2]*Faculty of Engineering and Surveying, University of Southern Queensland, Toowoomba, Australia*

ABSTRACT

We describe the X-series impulse facilities at The University of Queensland and show that they can produce useful high speed flows of relevance to the study of high temperature radiating flow flields characteristic of atmospheric entry. Two modes of operation are discussed: (a) the expansion tube mode which is useful for subscale aerodynamic testing of vehicles and (b) the non-reflected shock tube mode which can be used to emulate the nonequilibrium radiating region immediately following the bow shock of a flight vehicle.

Key words: expansion tube; nonreflected-shock tube.

1. INTRODUCTION

The regions of high speed flight normally associated with significant gaseous radiation are in the upper atmosphere, where the low density makes it difficult to reproduce such flows in ducted facilities, such as shock tubes. Radiating flows can be generated in expansion tubes and may be of sufficient duration to form steady flows around subscale flight vehicle models as shown in Figure 1(a), but experiments have to be performed at higher than flight densities and require scaling to interpret the results. As radiant heat transfer does not follow the normal density-length scaling procedures used for wind-tunnel testing, full similarity with the flight conditions is not obtained. In particular, the ratio of convective to radiative heat transfer is different in flight, as is the coupling of the radiation to the flow field. Typical geometric scale factors range from tens to thousands, indicating that the density levels required for approximate flow similarity in the simulations have to be higher than flight levels by the same sort of factors. Experimental aerodynamic tests of this nature are still worth doing because the techniques for studying radiating hypersonic flows can be developed and validated.

To investigate the fundamental radiation parameters in shock-heated flows, conditions close to real flight densities are also required. Experiments could focus on the region immediately behind the bow shock of the vehicle. This region contains the nonequilibrium radiating zone which is characteristically short, ranging from a few tens of millimetres for small capsules, up to several hundred millimetres for upper atmosphere ballute applications. Suitable flow conditions can be achieved in nonreflected shock tunnels as shown in Figure 1(b), but the low Reynolds numbers lead to rapid boundary layer growth and severely limit the amount of shock-heated test gas that can be generated. Flow slug lengths are typically less than a tube diameter and scale in proportion to the density and the square of the tube diameter. Tunnels suitable for the study of low density, high speed flow therefore require large bores and powerful drivers.

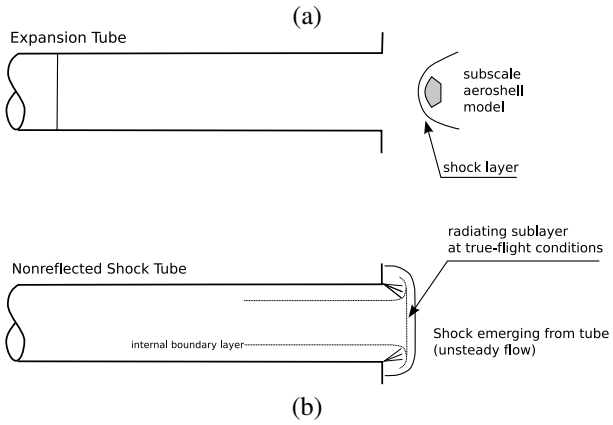

Figure 1. Layout of the experiments (a) aerodynamic testing of a subscale aeroshell, (b) flow behind a bow shock with full physical similarity to flight.

2. THE UQ FACILITIES

The X1, X2 and X3 impulse facilities (Table 1) are free-piston driven expansion tubes which can produce flows at super-orbital speeds, up to 15 km/s [10]. Figure 2 shows the X2 facility as it is used with the driven tube connected directly to the test-section.

Depending on the mode of operation, the driven tube

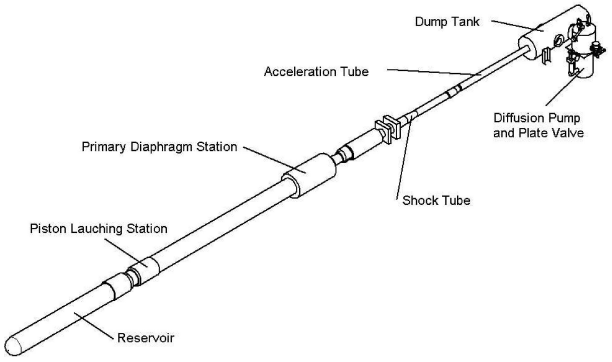

Figure 2. The X2 super-orbital impulse facility [11].

configuration will change. For expansion tube operation, the driven tube will consist of a shock tube and an acceleration tube, of equal cross-sectional areas, separated by a light plastic diaphragm. For nonreflected shock tube operation the driven tube will be just a shock tube. In both cases, the free-piston compressor is coupled to the upstream-end of the shock tube at the primary diaphragm station. The primary diaphragm is a heavy, steel diaphragm which regulates the pressures experienced within the tubes during operation.

Table 1. Super-orbital impulse facilities at The University of Queensland.

	Facility		
	X1	X2	X3
overall length (m)	12	20	65
driven-tube bore (mm)	38	85	183
driven-tube length (m)	5	8	36
piston mass (kg)	4	35	470

3. EXPANSION TUBE MODE

For testing of subscale aeroshell models, the facility is operated in expansion tube mode. The process is shown on the space-time diagram in Figure 3. An example X2 operating condition, relevant to atmospheric entry to Titan, is labelled as shot x2s97 in Table 2.

Although the zero on the time-axis of the space-time diagram is at main diaphragm (Figure 3) rupture, the piston has been in motion for approximately 80 ms as it accelerated along the compression tube and compressed the driver gas. Upon primary-diaphragm rupture, a strong shock is driven through the test gas, raising its pressure and temperature and accelerating it up to a speed of 2.7 km/s. This shock reaches the secondary diaphragm which is shattered and left behind in the boundary layer along the acceleration tube. The test gas flowing into the

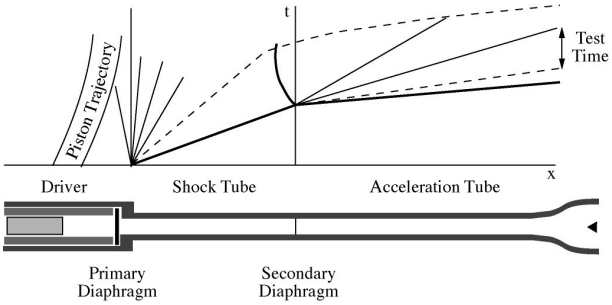

Figure 3. Schematic diagram of the X2 facility, with nozzle, operating in expansion tube mode.

acceleration tube expands to final test-flow conditions as it approaches the test-section. The amount of expansion of the test gas is regulated by the initial acceleration-gas pressure and the profile of the nozzle at the downstream-end of the acceleration tube [11].

3.1. Estimation of Operating Conditions

The numerical simulation of the facility is an important part of characterising the free-stream flow that is applied to the aeroshell model. The condition of free-stream flow is estimated from a mix of direct measurements and calculations. Operating parameters that can be directly measured are the initial fill pressures and temperatures, the shock speeds, Pitot pressures at the end of the nozzle and static pressures at a number of locations along the driven tube and expansion nozzle. The overall numerical simulation is a combination of a one-dimensional simulation of the high-pressure sections of the facility with an axisymmetric simulation of the low-pressure acceleration tube and nozzle. The transient, one-dimensional flow data just upstream of the secondary diaphragn is used as inflow to the subsequent axisymmetric simulation.

The flow through to the end of the shock tube is simulated with the L1d code [4]. Chemical equilibrium (using thermochemical data from the CEA program [5]) is usually assumed for this part of the facility because, in regions where the gas temperature is high, the pressure is also high. The one-dimensional nature of the simulation to the downstrean-end of the shock tube is also considered adequate because the boundary layers are relatively thin.

In contrast, expansion of the test flow through the acceleration tube and nozzle exhibits strong chemical-nonequilibrium and viscous effects. A viscous axisymmetric calculation using the MB_CNS code [3] is used to estimate the flow development down the acceleration tube and through the nozzle. The multidimensional nature of the test flow is highlighted in Figure 4 which shows the contours of pressure at an instant during the test flow period. The core flow is at quite different conditions to flow near the nozzle walls, as would be expected with a shock appearing within the plotted pressure field.

Table 2. Initial (fill) conditions. Gas compositions are given as volume fractions. Initial temperatures are assumed to be room temperature, approximately 23°C.

	Shot Identity			
	x2s97	x3s296	x3s346	x3s347
compressed-air pressure (MPa)	1.75	1.54	1.54	1.54
primary-diaphragm thickness (mm)	1.6	1.6	1.6	1.6
driver-gas composition	0.665 He+0.335 Ar	0.8 He+0.2 Ar	1.0 He	1.0 He
driver-gas pressure (kPa)	48	18.8	18.7	18.7
buffer-gas composition	–	–	1.0 He	1.0 He
buffer-gas pressure (kPa)	–	–	3.2	3.2
test-gas composition	0.95 N_2+0.05 CH_4	0.95 N_2+0.05 CH_4	air	air
test-gas pressure	29 kPa	2.2 kPa	10 Pa	3 Pa
secondary-diaphragm thickness (mm)	0.025	0.025	0.013	0.013
acceleration-gas composition	air	air	–	–
acceleration-gas pressure (Pa)	14	5.5	–	–

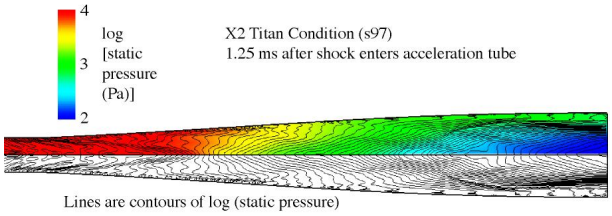

Figure 4. Pressure field in the nozzle during the test period.

Figure 5 compares the simulated data with the measured pressure from a transducer embedded in the wall near the exit plane of the nozzle. Agreement is good, particularly for the magnitude and duration of the pulse associated with the starting shock structure that is pushed through the nozzle, and then for the subsequent arrival of the unsteady expansion.

Despite the presence of the shock near the nozzle walls (Figure 4), the core flow conditions, as shown in Figure 6, are reasonably steady and are maintained for a useful length of time of nearly 100 μs. Note that the pressure in the core is approximately 113 Pa, about one tenth of the pressures observed near the nozzle wall. The other estimated flow parameters are $M = 18.7$, $\rho = 1.69 \times 10^{-3}$ kg/m^3, $u = 5.72$ km/s and $T = 210$ K.

Because the unsteady expansion of the early part of the test gas is rapid, the chemical species tend to be frozen at conditions not far from the high-temperature composition that existed in the shock tube. Core-flow mass fractions for this simulation are estimated as N_2:0.9452, CH_4:3.101×10^{-5}, CH_3:8.878×10^{-8}, CH_2:2.810×10^{-9}, CH:1.492×10^{-9}, C_2:3.441×10^{-9}, H_2:5.472×10^{-3}, CN:3.274×10^{-7}, NH:6.096×10^{-13}, HCN:4.924×10^{-2}, N:4.688×10^{-17}, C:1.092×10^{-9},

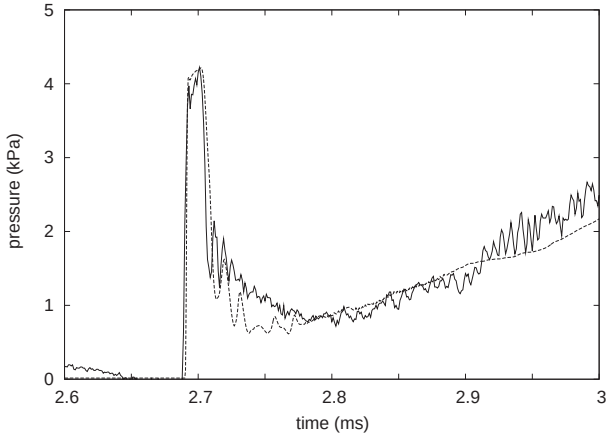

Figure 5. History of static pressure at the wall, at nozzle exit. The solid line is measured data while the dashed line is data from the numerical simulation. The zero of the time axis is at secondary-diaphragm rupture. Some low-frequency background noise appears on the measured signal and is particularly noticeable at $t = 2.6$ms.

and H:3.737×10^{-5}. Agreement with the measured Pitot pressure is not particularly good (Figure 6), with the low simulation values being consistent with the shock speed being about 5% lower than that measured in the facility [1]. This was, however, a low resolution simulation and we shall be running future simulations with higher resolution grids.

3.2. Radiant Heat Flux Measurement

Heat flux measurements have been made on a subscale Pathfinder aeroshell model in a gas mix that simulated Titan's atmosphere. The radiant heat-flux sensors consisted

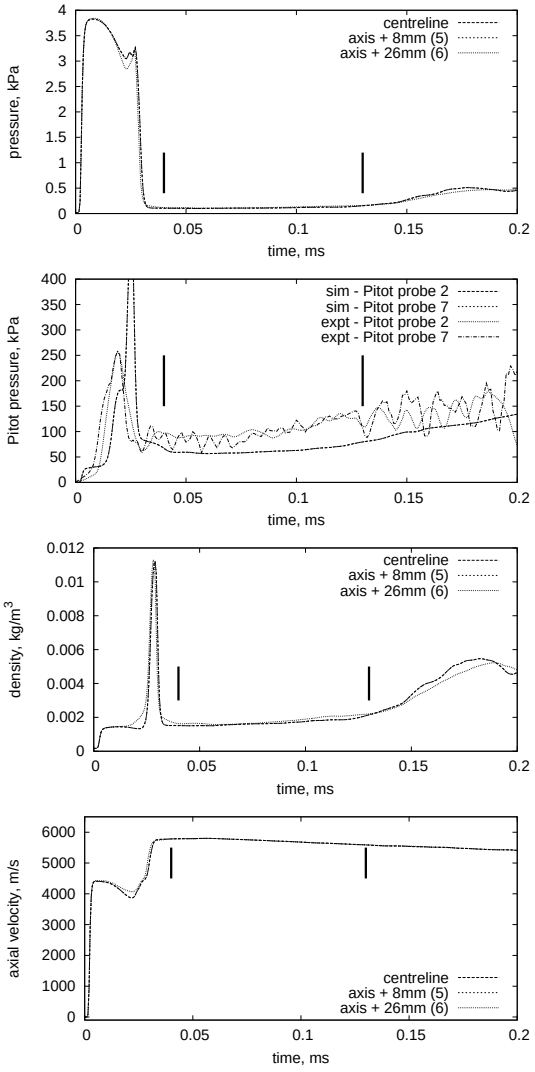

Figure 6. Conditions near the nozzle centerline at the exit plane. The zero of the time axis is aligned with the arrival of the shock and the vertical bars indicate the estimated start and end of the test period.

of pairs of thin-film heat transfer gauges mounted behind quartz windows [2]. Embedded in the aeroshell surface, adjacent to the radiation sensor were two thermocouples which were exposed to the combined radiant and convective heat load. Figure 7 shows the response of these sensors for a single shot in the X3 facility. Shots with and without CH_4 in the test gas showed clearly that significant radiation occurred only when CH_4 was present (Figure 8).

3.3. Optical Imaging

Using the second and third harmonics from a Nd:YAG laser (532 nm & 355 nm), a holographic technique [7] was used to produce interferometric images for the flow of nitrogen around a 15 mm cylinder in a flow with

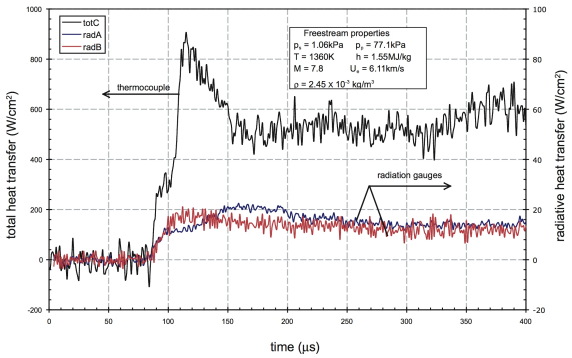

Figure 7. Total heat flux history for shot x3s294 with the Pathfinder aeroshell model.

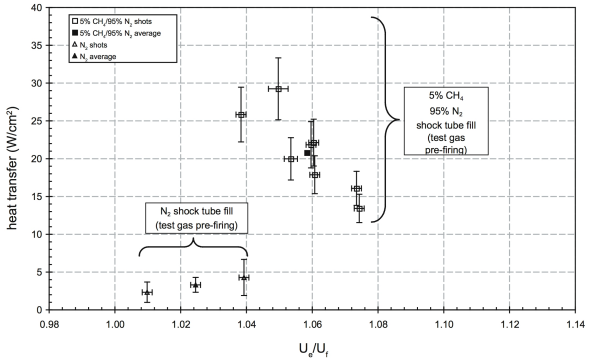

Figure 8. Radiative heat flux measurements for the Pathfinder aeroshell model for a number of shots.

free-stream density 0.0014 kg/m^3 and velocity 10.3 km. The interferograms were processed using Fourier transform and unwrapping techniques to determine the fringe shift at each point and this process gave the distributions shown in Figures 9 and 10 [6]. Agreement with computational data from the LAURA code [8] is good.

4. NONREFLECTED SHOCK TUBE MODE

For emulating the nonequilibrium radiation region following a bow shock, the X3 facility is operated in nonreflected shock tube mode with the process shown in Figure 11. Note that the test period is associated with the gas immediately following the primary shock as it enters the test section.

Example X3 operating conditions, relevant to earth atmospheric reentry and the FIRE II experiments, are labelled as shots x3s346 and x3s347 in Table 2. These conditions provide shock speeds of 8.4 km/s and 9.6 km/s, respectively. Operation of the facility in this nonreflected shock tube mode is similar to the expansion tube mode but the test gas is now initially filling the region downstream of the secondary diaphragm and into the test section. The

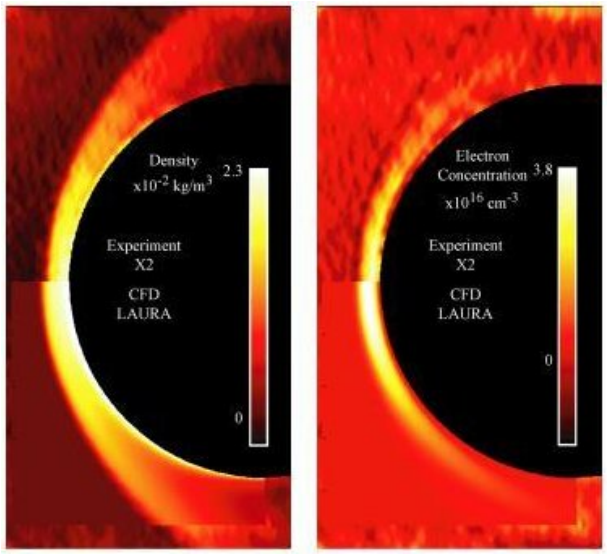

Figure 9. Density and electron concentration around a 15 mm cylinder. The computational data is overlaid on the lower half field of each image.

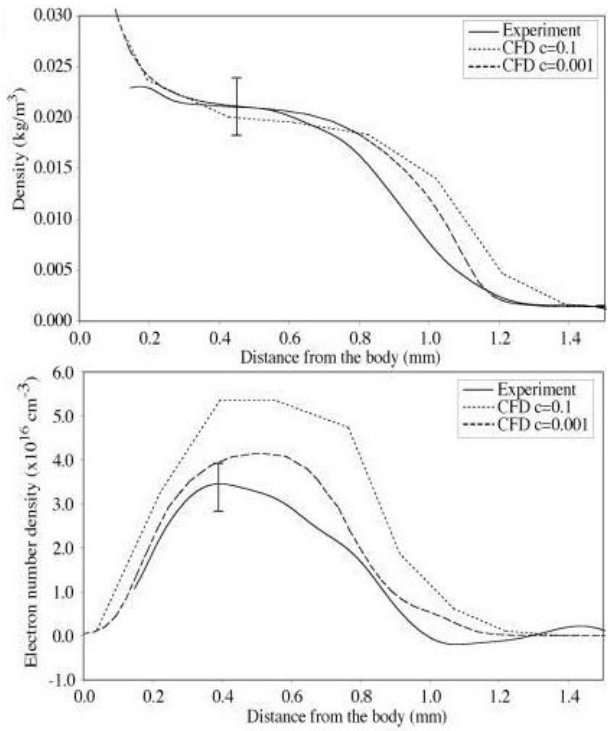

Figure 10. Density and electron concentration along the stagnation line for a 15 mm cylinder. The shock is located at approximately 1 mm from the body.

medium density gas between the primary and secondary diaphragms is a secondary, shock-heated driver and acts as a buffer between the test gas and the jet of driver gas that is produced during the rupture of the primary diaphragm. The rupture of the secondary diaphragm is rapid and more uniform across the diameter of the tube

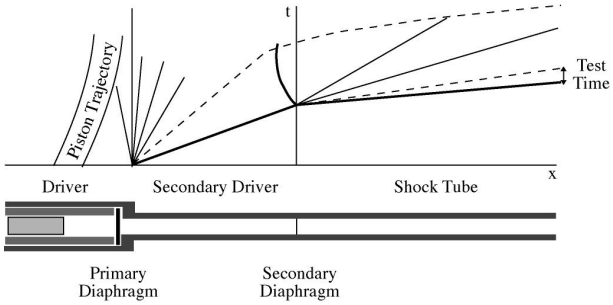

Figure 11. Schematic diagram of the X3 facility operating in nonreflected shock tube mode.

[12].

Figures 12 and 13 show the histories of static pressure at a point close to the downstream-end of the driven tube and a Pitot pressure signal from the core flow, a little further downstream, in the test section. The slow rise of the signals is characteristic at low operating pressures (and is not helped by the low sampling rate that was used for these particular shots). The estimated test period is identified on each of the Pitot pressure signals and the time between the arrival of the primary shock and the subsequent arrival of the contact surface. At these speeds, we are seeing 200 mm and 100 mm slugs of test gas with the current facility and, with an increase to a 500 mm bore driven tube, we should see substantially longer test slugs [9].

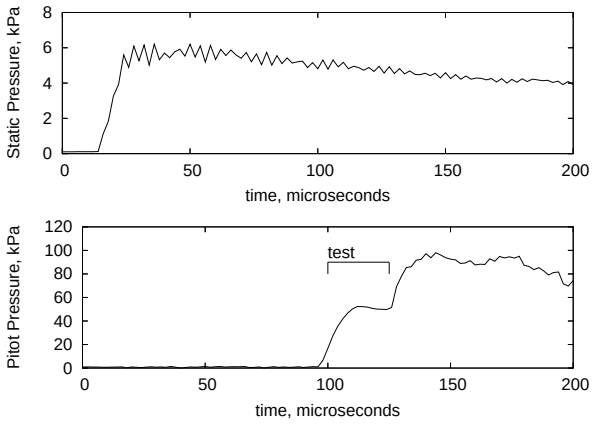

Figure 12. Wall static pressure at the end of the driven tube and Pitot pressure history in the test section for shot x3s346.

5. CONCLUDING REMARKS

The X-series of impulse facilities are capable of producing high-speed test conditions suitable for the study of high-temperature radiating flow. Experiments on subscale aeroshell models may be undertaken using the expansion-tube mode of operation while direct simulation of the nonequilibrium radiation region behind the

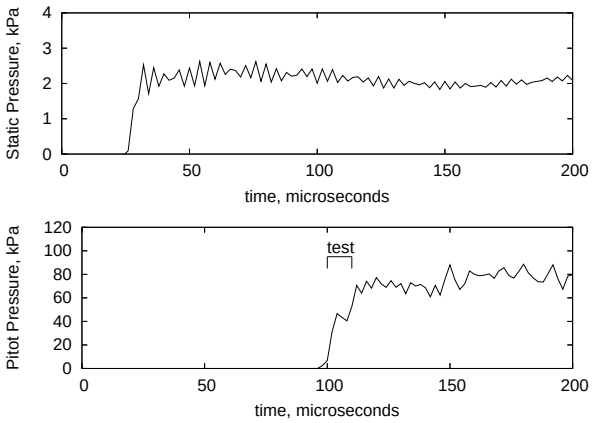

Figure 13. Wall static pressure at the end of the driven tube and Pitot pressure history in the test section for shot x3s347.

bow shock of the flight vehicle can be achieved with the nonreflected shock tube mode of operation. Preliminary experiments and whole-of-tube calculations have been undertaken for a few conditions but further conditions need to be explored and refined calculations need to be made.

ACKNOWLEDGMENTS

This project has been supported, for both development of the expansion tube facilities and of our computational facility, by the Smart State Research Facilities Program of the Queensland State Government, and by the Australian Research Council. Many of the graduate students have been supported by Australian Government Postgraduate Research scholarships.

REFERENCES

1. A. Brandis, R. J. Gollan, M. Scott, R. G. Morgan, P. A. Jacobs, and P. Gnoffo. Expansion tube operating conditions for studying non-equilibrium radiation relevant to Titan aerocapture. In *42nd AIAA/ASME/SAE/ASEE Joint Propulsion Conference and Exhibit*, AIAA-Paper-2006-4517. American Institute of Aeronautics and Astronautics, July 2006.

2. B. R. Capra. Aerothermodynamic simulation of subscale models of the FIRE II and Titan Explorer vehicles in expansion tubes. PhD Thesis, The University of Queensland, Brisbane, August 2006.

3. P. A. Jacobs. MB_CNS: A computer program for the simulation of transient compressible flows; 1998 Update. Department of Mechanical Engineering Report 7/98, The University of Queensland, Brisbane, June 1998. http://www.mech.uq.edu.au/cfcfd/.

4. P. A. Jacobs. L1d: a computer program for the simulation of transient-flow facilities. Department of Mechanical Engineering Report 1/99, The University of Queensland, Brisbane, Australia., January 1999. http://www.mech.uq.edu.au/cfcfd/.

5. B. J. McBride and S. Gordon. Computer program for calculation of complex chemical equilibrium compositions and applications II. Users manual and program description. Reference Publication 1311, NASA, June 1996.

6. T. J. McIntyre, A. I. Bishop, H. Rubinsztein-Dunlop, and P. A. Gnoffo. Experimental and numerical studies of ionizing flow in a super-orbital expansion tube. *A.I.A.A. Journal*, 41(11):2157–2161, 2003.

7. T. J. McIntyre, M. J. Wegener, A. Bishop, and H. Rubinsztein-Dunlop. Simultaneous two-wavelength holographic interferometry in a super-orbital expansion tube facility. *Applied Optics*, 36:8128–8134, 1997.

8. F. McNeil Cheatwood and P. A. Gnoffo. User's manual for the Langley Aerothermodynamic Upwind Relaxation Algorithm (LAURA). Technical Momorandum 4674, NASA Langley Research Center, Hampton, Virginia, April 1996.

9. R. G. Morgan, T. J. McIntyre, R. J. Gollan, P. A. Jacobs, A. Brandis, M. McGilvray, D. van Diem, P. Gnoffo, M. Pulsonetti, and M. Wright. Radiation measurements in nonreflected shock tunnels. In *25th AIAA Aerodynamic Measurement Technology and Ground Testing Conference*, AIAA-Paper-2006-2958. American Institute of Aeronautics and Astronautics, June 2006.

10. A. J. Neely and R. G. Morgan. The superorbital expansion tube concept, experiment and analysis. *The Aeronautical Journal*, 98(973):97–105, 1994.

11. M. P. Scott, P. A. Jacobs, and R. G. Morgan. Nozzle development for an expansion tunnel. In Jiang, editor, *24th International Symposium on Shock Waves, Beijing, China*. Springer, July 2004.

12. M. Wegener, M. A. Sutcliffe, and R. G. Morgan. Optical study of a light diaphragm rupture process in an expansion tube. *Shock Waves*, 10(3):167–178, 2000.